PAPER

Fabrication of electroactive oligoaniline functionalized poly(amic acid) nanofibers for application as an ammonia sensor

Shutao Wang,[a] Danming Chao,*[a] Erik B. Berda,[b] Xiaoteng Jia,[a] Rui Yang,[a] Xitao Wang,[a] TingTing Jiang[a] and Ce Wang*[a]

A novel, well-defined, multifunctional electroactive poly(amic acid) (EPAA) containing oligoaniline pendants was synthesized by a one-step synthetic route. The structure was confirmed spectroscopically *via* nuclear magnetic resonance (NMR) and Fourier-transform infrared (FTIR) spectra, and the thermal stability was probed *via* thermogravimetric analysis (TGA). The oligoaniline pendants imparted excellent electroactivity, photoresponsiveness to chemical redox and electrochemical modulation, and expectable electrochromic performance to the obtained EPAA. Leucoemeraldine base EPAA (LEPAA), emeraldine base EPAA (EEPAA) and HCl-doped emeraldine base EPAA (HCl-doped EEPAA) nanofibers were fabricated by electrospinning and were characterized by scanning electron microscopy (SEM) to test their morphology, and a contact angle goniometer was used to test their hydrophilicity. The as-prepared HCl-doped EEPAA nanofibers were then evaluated for their ability to sense ammonia.

Introduction

As an important conducting polymer, polyaniline (PANI) is particularly attractive due to its simple polymerization, environmental stability, and the affordability of the requisite raw materials.[1,2] These attributes ideally suit PANI and its related copolymers for application in metal anticorrosion,[3] electrochromic materials,[4,5] electromagnetic shielding materials,[6] microwave absorbtion[7] and chemical sensing.[8,9] However, successful commercial applications of PANI are hampered by poor solubility in common solvents.[10] Moreover, the structural defects of PANI hinder thorough microstructure characterization and prevent a mechanistic understanding of conduction in these materials.[11,12] The drawbacks related to PANI can be solved by incorporating an aniline oligomer (oligoaniline) into other polymeric systems. Due to the oligoanilines' favourable solubility, precise molecular structure and unique optical and electrical properties, this strategy has been preferentially applied to synthesize a number of multifunctional polymers. By modulating such features as the mole percent of oligoaniline incorporation or the number of oligomeric repeating units, the desired properties of the resultant material can be precisely tuned. Because of this, polymers containing oligoaniline segments continue to receive

extensive interest and attention. Chen *et al.*[13] synthesized a biodegradable and electroactive polymer as the scaffold for tissue engineering through the polycondensation of hydroxyl-capped poly(L-lactide) and a carboxyl-capped aniline penta-mer. The polymer possessed properties favorable for use *in vivo* as a nerve repair scaffold. Yeh *et al.*[14] obtained an aniline-pentamer-based electroactive polyimide (EPI) by oxidative coupling polymerization. The EPI exhibited excellent corrosion protection when applied to cold-rolled steel (CRS) electrodes. The mechanism for this enhanced corrosion protection of EPI coatings on the CRS electrode was also proposed. Jia *et al.*[15] prepared a series of novel electroactive copolymers of poly(amic acid) (PAA) bearing pendant aniline tetramer groups *via* direct polycondensation from a novel electroactive dia-mine, 4,4′-diaminodiphenyl ether and 3,3′,4,4′-biphenyltetra-carboxylic dianhydride. This material exhibited an extremely high optical contrast, moderate coloration efficiency and short switching times.

Electrospinning is an effective technique to fabricate nanofibers with a high surface-to-volume ratio, high aspect ratios and controllable diameters. So called electrospinning nanofibers are widely applicable in areas such as filtration, catalysis, and chemical and biological sensing, owing to their low dimensions and large surface areas.[16–23] Recently, focus has shifted toward the preparation of gas sensors based on nanofibers containing a PANI component, which possess a high sensitivity and fast response time compared with the customary bulk and/or thin film PANI materials. Zampetti *et al.*[24] fabricated three different conducting composite

[a] *Alan G. MacDiarmid Institute, College of Chemistry, Jilin University, Changchun, 130012, P. R. China. E-mail: chaodanming@jlu.edu.cn; cwang@jlu.edu.cn; Fax: +86-431-85168292; Tel: +86-431-85168292*

[b] *Department of Chemistry and Materials Science Program, University of New Hampshire, Durham, New Hampshire 03824, USA*

nanofibers (PVP-PANI, PS-PANI, PEO-PANI) where PVP, PS, and PEO were used as carriers for the conducting polymer. The composite nanofibers revealed a good response to NH_3 and NO_2. Li et al.[25] prepared PANI–TiO_2 composite nanofibers, where the TiO_2 filaments prepared by electrospinning acted as a base and the PANI nanofibers were anchored to the surface of the as-prepared TiO_2 nanofibers by the oxidation of Mn_2O_3. These composite nanofiber sensors expressed a readable response to ammonia even at concentrations as low as 25 ppb.

To the best of our knowledge there are no reports in the literature of oligoaniline-containing polymers used as gas sensing materials. We demonstrate here an efficient, one-step synthetic route to a novel EPAA containing aniline tetramer groups as pendants. Due to its excellent solubility, the obtained EEPAA was electrospun into nanofibers, which were used as an ammonia sensor material. The ammonia sensor was evaluated carefully and these results are likewise discussed in detail.

Experimental

Materials

All chemicals, including 4-aminophenol (99%), dichloromethane (99.5%) and 4,4′-oxydiphthalic anhydride (ODPA, 98%) were purchased from Shanghai Chemical Factory. N,N′-dimethyla-cetamide (DMAc, 99%), N,N′-dimethylformamide (DMF, 99%), dimethyl sulfoxide (DMSO, 99%), N-methyl-2-pyrrolidone (NMP, 99%), tetrahydrofuran (THF, 99%) and toluene (99%) were used as received without further purification. Anhydrous potassium carbonate was dried at 110 °C for 24 h before use. Distilled and deionized water was used. Optically transparent indium–tin oxide (ITO) glass substrates (Reintech electronic technologies Co. Ltd, Beijing) with dimensions of 4.0 cm × 0.6 cm were used as the electrochromic thin film electrode.

Measurements

Fourier-transform infrared spectra (FTIR) measurements were recorded on a Bruker vector 22 spectrometer. Nuclear magnetic resonance spectra (NMR) of EPAA in deuterated dimethyl sulfoxide (DMSO) were recorded on a Bruker-500 spectrometer. Mass spectroscopy (MS) was performed on an AXIMA-CFR laser desorption ionization flying time spectro-meter (COMPACT). The number-average molecular weight (M_n), weight-average molecular weight (M_w), and molecular weight distribution of the polymer were measured with a gel permeation chromatography (GPC) instrument equipped with a Shimadzu GPC-802D gel column and a SPD-M10AVP detector with THF as an eluent at a flow rate of 1 mL min^{-1}. UV-vis spectra were performed on a UV-2501 PC Spectrometer (SHIMADZU) in DMAc. A Perkin-Elmer PYRIS 1 TGA was used to investigate the thermal stability of EPAA. Cyclic voltammetry (CV) was investigated on a CHI 660A electrochemical work-station (CH instruments, USA) with a conventional three-electrode cell, using a saturated calomel electrode (SCE) as the reference electrode, a platinum wire electrode as the counter electrode, and a glassy carbon electrode (GCE, Φ 3.0 mm) as the working electrode. Spectroelectrochemical measurements were carried out in a cell built from a 1 cm commercial cuvette using a UV-2501 PC Spectrometer (SHIMADZU). The ITO-coated glass was used as the working electrode, a Pt wire as the counter electrode, an Ag/AgCl cell as the reference electrode and 1.0 mol L^{-1} H_2SO_4 was used as the electrolyte. Static contact angles of water on the three different films were measured with a JC2000C2 contact angle goniometer (Shanghai Zhongchen Powereach Company, China) by the sessile drop method with a micro syringe at room temperature. The morphology of the nanofibers was characterized via scanning electron microscopy (SEM, SHIMADZU, SSX-550, Japan).

Synthesis of electroactive diamine monomer (EDA)

The synthetic route of EDA has been reported in the literature.[15]

MALDI-TOF-MS: m/z calculated for $C_{43}H_{36}N_6O_3$ = 684.8. Found 685.0. FTIR (KBr, cm^{-1}): 3380 (s, v_{N-H}), 3037 (m, v_{C-H}), 1657 (vs, $v_{C=O}$), 1602 (s, $v_{C=C}$ of benzenoid rings), 1506 (vs, $v_{C=C}$ of benzenoid rings), 1294 (s, v_{C-N}), 1233 (m, v_{C-O-C}), 829 (m, δ_{C-H}), 750 (m, δ_{C-H}), 696 (m, δ_{C-H}). ^{1}H NMR (500 MHz, d$_6$-DMSO, ppm): δ = 10.24 (s, 1H, due to –CONH–), δ = 7.74 (s, 1H, due to –NH–), δ = 7.69 (s, 1H, due to –NH–), δ = 7.60 (s, 1H, due to –NH–), δ = 7.54 (d, 2H, due to Ar–H), δ = 7.14 (t, 3H, due to Ar–H), δ = 6.93 (d, 12H, due to Ar–H), δ = 6.81 (d, 4H, due to Ar–H), δ = 6.67 (t, 1H, due to Ar–H), δ = 6.59 (d, 4H, due to Ar–H), δ = 6.29 (d, 2H, due to Ar–H), δ = 4.99 (s, 4H, due to –NH$_2$).

Synthesis of 1,3-bis(3-aminophenoxy-4′-benzoyl)benzene (BABB)

The synthetic method for BABB was conducted according to previous literature.[26]

MALDI-TOF-MS: m/z calculated for $C_{32}H_{24}N_2O_4$ = 500. Found 501.1. FTIR (KBr, cm^{-1}): 3465 (s, v_{N-H}), 3360 (s, v_{N-H}), 1601 (vs, $v_{C=O}$), 1481 (s, $v_{C=C}$ of benzenoid rings), 1250 (s, v_{C-N}), 1149 (m, v_{C-O-C}), 975 (m, δ_{C-H}), 844 (m, δ_{C-H}), 732 (m, δ_{C-H}). ^{1}H NMR (500 MHz, d$_6$-DMSO, ppm): δ = 8.0 (d, 2H, due to Ar–H), δ = 7.9 (s, 1H, due to Ar–H), δ = 7.8 (d, 4H, due to Ar–H), δ = 7.7 (t, 1H, due to Ar–H), δ = 7.1 (m, 6H, due to Ar–H), δ = 6.4 (d, 2H, due to Ar–H), δ = 6.3 (s, 2H, due to Ar–H), δ = 6.2 (d, 2H, due to Ar–H), δ = 5.3 (s, 4H, due to –NH$_2$).

Synthesis of EPAA

We adopted a one-step synthetic route to obtain the EPAA copolymer. The typical procedure is as follows: EDA (0.342 g, 0.5 mmol), BABB (1.000 g, 2.0 mmol), ODPA (0.775 g, 2.5 mmol) and DMAc (5.25 mL) were added into a 25 mL three-necked flask. The mixed solution was stirred for 5 h with magnetic stirring under nitrogen at room temperature. Hence, we got an EPAA solution, whose solid content was 30 wt%. The synthetic procedure for EPAA is shown in Scheme 1.

Preparation of LEPAA, EEPAA and HCl-doped EEPAA nanofibers

The as-prepared solution was then loaded into a glass syringe equipped with a needle 1 mm in diameter at the tip. The needle was connected to a high-voltage supply that is capable of generating DC voltages up to 30 kV. In our experiment, a voltage of 15 kV was applied for electrospinning. A piece of flat
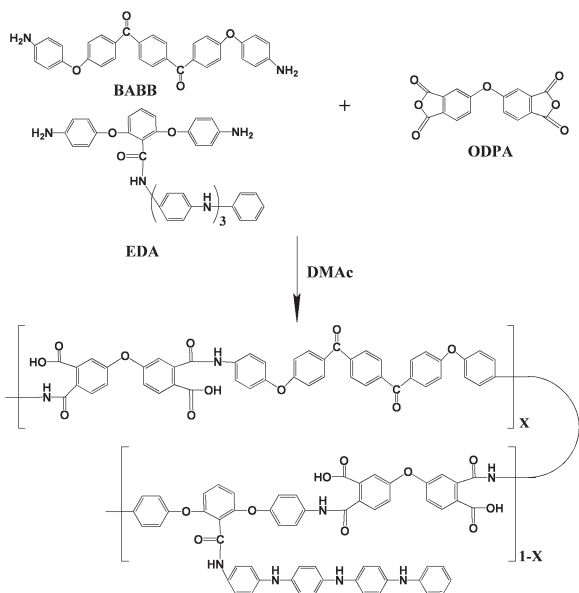
Scheme 1 Synthetic route of EPAA.

aluminium foil was placed 20 cm from the tip of the needle to collect the LEPAA nanofibers.

0.065 g $(NH_4)_2S_2O_8$ and 0.85 mL DMAc were added to 4 g as-prepared LEPAA solution under vigorous stirring for 4 h. We then obtained a green EPAA solution with a solid content of 25 wt%. EEPAA electrospun nanofibers were prepared by the same procedure as above. Finally, the nanofibers were peeled off the collector and doped by immersion into 1 M HCl for 3 h to obtain HCl-doped EEPAA nanofibers.

Fabrication of electrochromic electrodes

The ITO substrates were washed ultrasonically in DMAc for 30 min and then in ethanol for another 30 min, followed by drying in air before use. The EPAA solution (0.5 mL of the original solution diluted in 1 mL DMAc) was filtered through a 0.2 μm poly(tetrafluoroethylene) syringe filter, then spin-coated onto the ITO substrates. The spin-coating process started at 500 rpm for 9 s and then 1000 rpm for 30 s.

Ammonia sensing measurements

The as-prepared HCl-doped EEPAA nanofiber membrane (about 10 μm thick) was pasted in a ceramic substrate (7 mm × 5 mm × 0.5 mm) with three pairs of carbon interdigital electrodes followed by drying for 5 h in air at room temperature. To test the gas sensitivity of the nanofibers, the sensor was placed in a CGS-1 intelligent test system (Beijing Elite Tech Co. Ltd., Beijing, China), which is a sealed test box (about 20 L in volume). NH_3 was injected into the test box by a syringe through a rubber plug. The sensitivity R is defined as $R = (R_g - R_a)/R_a$, where R_a is the initial resistance before injecting NH_3 and R_g is the balance resistance after being exposed to a certain concentration of NH_3.[27] The times taken by the sensor to achieve 90% of the total resistance change were defined as the response time in the case of

adsorption and the recovery time in the case of desorption, respectively.[28]

Results and discussion

EPAA structures and thermal properties

The chemical structure of EPAA was confirmed *via* FTIR and ^{1}H NMR spectroscopy. FTIR spectra of EPAA displayed a characteristic peak at 3427 cm^{−1} corresponding to the N–H stretching vibration and at 3072 cm^{−1} due to the O–H stretching vibration of carboxylic acid groups. Characteristic absorption bands at 3029 cm^{−1} based on the C–H stretching vibration of aryl groups are present, as well as a peak due to the C=O stretching vibration at 1724 cm^{−1}. The stretching vibration of C=C of the benzene rings, located at 1593 cm^{−1} and 1503 cm^{−1}, is also present. A peak at 1308 cm^{−1} is attributed to the stretching vibration of C–N from the aniline tetramer segment. The vibration at around 1255 cm^{−1} was assigned to the stretching vibration of C–O–C of the aryl ether linkages. In the ^{1}H NMR of EPAA, the signals at $\delta = 13.13$ were ascribed to the hydroxyl protons of carboxylic acid groups, the signals around $\delta = 10.51$ were attributed to the amino protons of amide groups and the signals near $\delta = 7.98$ were assigned to the amino protons of oligoaniline. Moreover, other aromatic protons appeared at $\delta = 7.78$–7.54, $\delta = 7.49$–7.35 and $\delta = 7.27$–7.09. All of these ^{1}H NMR signals supported the expected molecular structure of EPAA. The M_n of Azo-PA-S-AT was found to be 3.13×10^4 with a polydispersity index (M_w/M_n) of 1.08. Moreover, EPAA exhibited outstanding solubility in polar solvents such as THF, DMF, DMAc, DMSO and NMP, likely due to the bulky pendant groups which can impede chain entanglement to some extent.

The thermal properties of EPAA were estimated by TGA (Fig. 1). The first stage mass loss beginning at 130 °C and ending at 270 °C was observed, corresponding to the progress of imidization and the concomitant evaporation of water. Decomposition of the main chain of the product of imidization occurred at 480 °C. This result highlights the outstanding thermal stability of EPAA, which features a much higher degradation temperature, after imidization, when compared with typical PANI materials.[29]
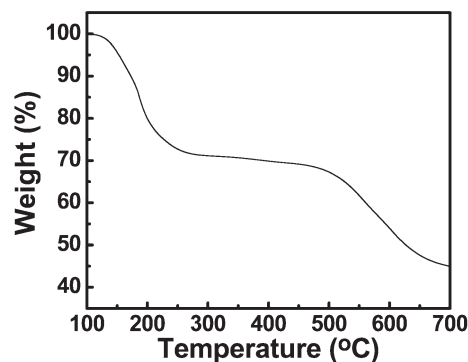
Fig. 1 TGA thermogram of EPAA in N_2.

Fig. 3 CV of EPAA electrodes in 1.0 mol L^{-1} H$_2$SO$_4$ at different potential scan rates: 20–200 mV s^{-1}. Inset shows the relationships between the oxidation peaks and reduction current *vs.* potential scan rate.
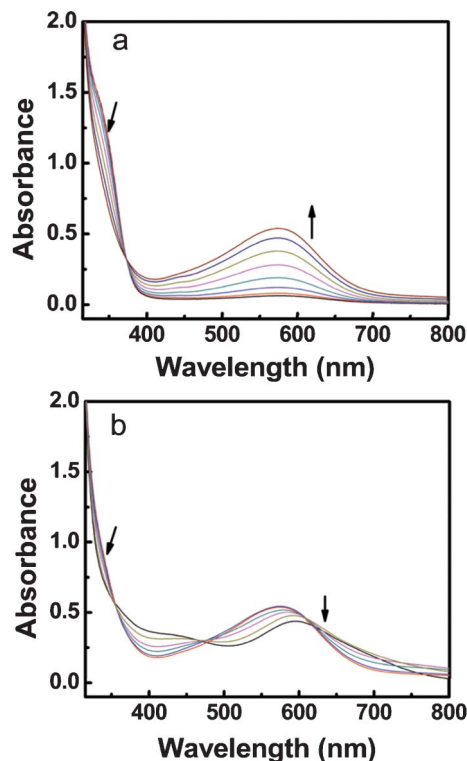
Fig. 2 UV-vis spectra monitoring the chemical oxidation of the EPAA. (a) From the leucoemeraldine oxidation state to the emeraldine oxidation state; (b) from the emeraldine oxidation state to the pernigraniline oxidation state.

Spectroscopic properties

The optical properties of EPAA were investigated by UV-vis spectroscopy. Fig. 2 presents the stepwise oxidization process of EPAA in DMAc when a trace amount of (NH$_4$)$_2$S$_2$O$_8$ was added into the solution. A gradual decrease in the absorption band from 350 nm to 315 nm, associated with π–π* transitions in oligoaniline segments, was observed upon oxidation. This is type of decrease in absorption is consistent with other PANI based materials.[30] The peak of this absorption cannot be readily assigned, however, because of the overlap of the π–π* transitions of the conjugated benzoid rings and the n–π* transitions of carbonyl groups connected with the benzene ring. Continued oxidation results in the emergence of a new absorption peak near 572 nm. This has be associated with the exciton-type transition between the HOMO orbital of the benzoid ring and the LUMO orbital of the quinoid ring.[31] When the intensity of the peak around 572 nm reached a maximum, the EPAA was in the emeraldine oxidation state with the parent aniline tetramer segment containing one quinoid ring. With further oxidization of EPAA, the absorption peak decreased and underwent a red shift. Finally, the absorption peak remained unchanged with further oxidation, which indicated that the EPAA had reached the pernigraniline oxidation state with the parent aniline tetramer segments containing two quinoid rings.

Electrochemical activity

The cyclic voltammetry of EPAA was shown in Fig. 3. During the test, the working electrode (prepared by casting the DMAc
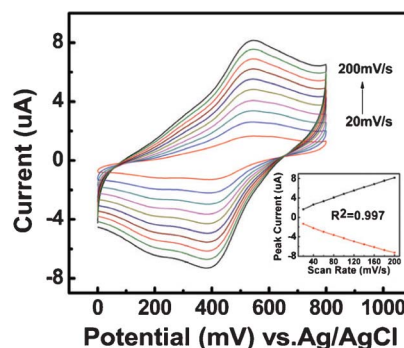
solution of EPAA on the GCE and evaporating to form a thin solid film), the reference electrode (a saturated calomel electrode (SCE)) and counter electrode (a platinum wire) formed a three-electrode system. Then they were examined in a strongly acidic electrolyte composed of 1.0 M H$_2$SO$_4$ (aq) solution at different potential scan rates (20–200 mV s^{-1}). The cyclic voltammetry of EPAA showed two redox processes. The reductive peaks at 206 mV corresponded to the emeraldine base (EB)–leucoemeraldine base (LEB) transition, while the reductive peaks at 387 mV showed the translation from pernigraniline base (PNB) to emeraldine base (EB). A linear dependence of the peak currents as a function of scan rates in the region 20–200 mV s^{-1} confirmed both a surface controlled process and a well-adhered electroactive polymer film.[32] The EPAA showed a good redox stability, which confirms the stability of the films and good adhesion between the polymer and working electrode.

Electrochromic performances

Spectroelectrochemical studies were performed on a film of EPAA spin-coated on the ITO glass slide in 1.0 mol L^{-1} H$_2$SO$_4$ coupled with applied potentials of -0.2, 0.2, 0.4, 0.8 and 1.0 V (*vs.* Ag/AgCl). Fig. 4 shows that the UV-vis absorption spectra of EPAA films varied with various applied potentials. The optical
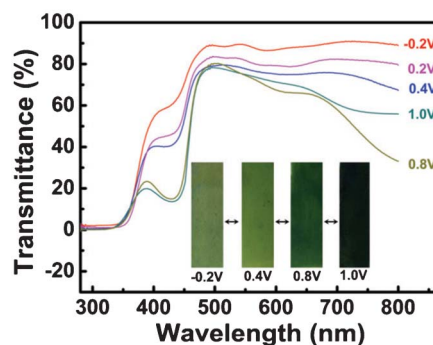
Fig. 4 Spectral changes of the EPAA electrode (0.6 × 3 cm^2) in 1.0 mol L^{-1} H$_2$SO$_4$ at different potentials. Inset shows photographs of the EPAA electrode at different potentials.
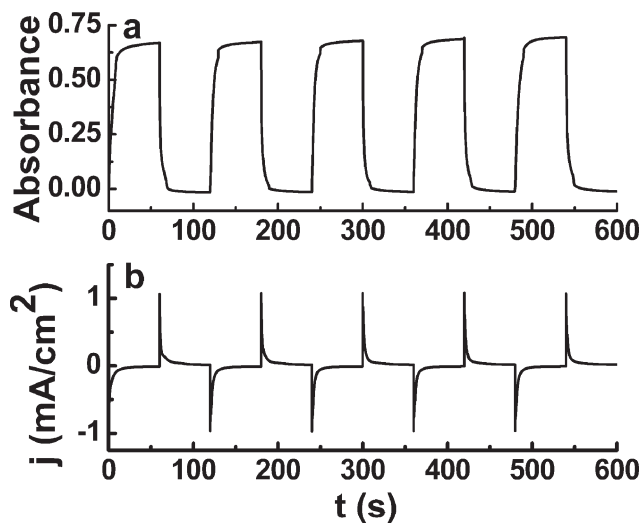
Fig. 5 (a) Absorbance change monitored at 700 nm of EPAA in 1.0 mol L^{-1} H$_2$SO$_4$ for the first 5 cycles and (b) current consumption.

constrast value (% ΔT), an important characteristic, was found to be 32.7% at 700 nm, measured between its colored (oxidization) and bleached (reduction) states. The color of the EPAA thin films changed from faint yellow (at -0.2 V), to kelly green (at 0.4 V), to green (at 0.8 V) and finally to absorptive invisible green (at 1.0 V). EPAA could have a wide application in electrochromic devices in light of its multicolor range from faint yellow to invisible green.

Apart from the optical constrast value (% ΔT), the switching time and the electrochromic efficiency are likewise important properties when evaluating electrochromic devices. The electrochromic performances of EPAA were recorded by spectrochronoamperometry in the optical contrast at 700 nm during repeated potential stepping between reductive (at -0.2 V) and oxidative (at 1.0 V) states with a residence time of 60 s. In Fig. 5, the switching times (defined as the time required to reach 95% of the full change in the coloring/bleaching process) are 12 s at 1.0 V for the coloring progress at 700 nm and 6 s at -0.2 V for bleaching. This is a somewhat slow switching rate for a conducting polymer electrochromic device, due mostly to the low concentration of conductive segments in the polymer structure. The electrochromic CE ($\eta = \Delta OD/Q$) was measured by monitoring the amount of ejected charge (Q) as a function of the change in optical density (ΔOD) of the polymer film. The electrochromic behavior of EPAA exhibited a CE up

to 94.7 cm^2 C^{-1} (at 700 nm) at the first oxidation stage. From the first 5 cycles presented in Fig. 5, we can conclude that the EPAA thin film exhibits a strong adherence to the ITO substrates and thus has excellent stability as an electrochromic device.

Morphology, hydrophilicity, and sensing properties of EPAA nanofibers

The morphologies of LEPAA, EEPAA and HCl-doped EEPAA nanofibers were characterized by SEM, which are shown in Fig. 6. The average diameters of LEPAA nanofibers ranged from 400 nm to 550 nm while the EEPAA nanofibers' average diameters were up to about 700 nm. After doping with HCl, the nanofibers remain constant without any change.

The surface hydrophilicity of these three different nanofibers were studied by measuring the static contact angle. The LEPAA nanofibers were quite hydrophobic, having a contact angle of 136.6°, while EEPAA was much more hydrophilic with a contact angle of 57.8°. The HCl-doped EEPAA completely wetted. These results are shown in Fig. 6. Clearly this is a function the synergistic effects of the pore structure and the surface energy of the nanofibers.

The sensing characteristics of PANI to ammonia, due to its reversible doping–dedoping properties, are well known. It can be predicted that EPAA will also possess good sensing properties due to the oligoaniline pendants. So, we tested the sensing properties to ammonia of the as-prepared HCl-doped EEPAA nanofibers. The HCl-doped EEPAA nanofibers' responsive behaviors to ammonia were investigated at room temperature (21 °C) with a relative humidity of 30%. Fig. 7 shows the sensitivities of the HCl-doped EEPAA nanofibers when they were exposed to different levels of NH$_3$ ranging from 1 ppm to 500 ppm. The results indicated clearly that the response increased rapidly with the increase of NH$_3$ below 100 ppm. The response increased slowly when the concentration of NH$_3$ was more than 100 ppm. Finally, the response reached a maximum value and didn't increase at an ammonia concentration of 400 ppm, confirming that no more active sites were available to react with NH$_3$. The responsive range of EPAA nanofibers was not as wide because of the low content percentage (20%) of the oligoaniline in the polymer structure. However, it could be modulated easily by increasing the concentration of the oligoaniline in the polymer architecture.

PANI transforms from an insulator to a p-type semiconductor when it is doped by protonic acids [HA + PANI = A$^-$ + PANIH$^+$]. Contrarily, when it is exposed to an alkali gas, PANIH$^+$ will reversibly transform from a semiconductor to an
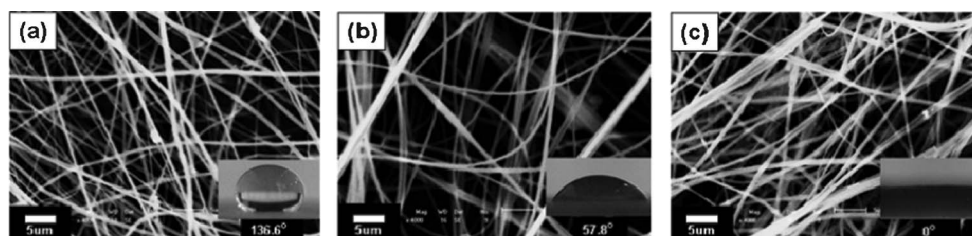
Fig. 6 SEM images of nanofibers prepared by (a) LEPAA, (b) EEPAA, (c) HCl-doped EEPAA and their water contact angles.
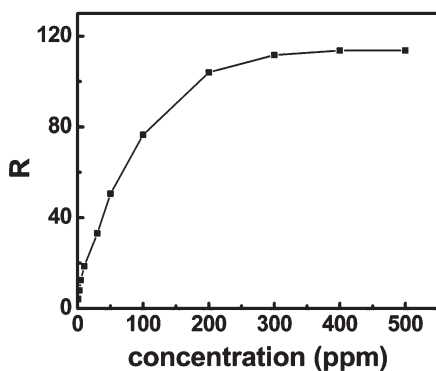
Fig. 7 Linear plot of the responses of the sensor based on HCl-doped EEPAA nanofibers to NH_3 in the range 1–500 ppm.

insulator [NH_3 + $PANIH^+$ = PANI + NH_4^+],[33] which leads to a sharp increase in resistance. Thus, PANI materials have a unique acid–base doping–dedoping reversibility. The response–recovery property is another important performance for evaluating chemical sensors, and this was investigated in our experiment. As shown in Fig. 8, the response time was 141 s and the recovery time was 92 s at an ammonia concentration of 30 ppm. Compared to some PANI sensors reported earlier,[34–36] the HCl-doped EEPAA nanofiber sensor in our study exhibits a faster response and shorter recovery time, due to its high surface-to-volume ratio.

Though the content of oligoaniline pendants in EPAA was low (20%), the nanofibers still exhibited a good response to ammonia, owing to their high surface-to-volume ratio. At the same time, they also revealed acceptable reversibly responsive behaviors. To meet the demands for commercial viability, a new polymer with a higher content percentage of oligoaniline is being prepared in our laboratory. Gas sensors with a high sensitivity and quick response should be reported in the future.
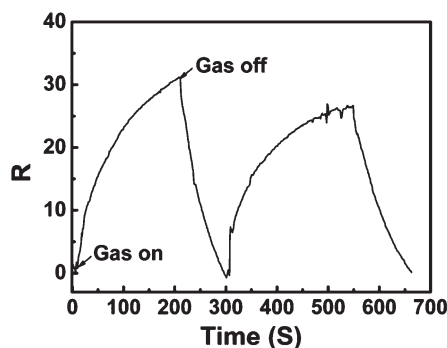
Fig. 8 The reversibly responsive behaviors of the HCl-doped EEPAA nanofibers to 30 ppm ammonia.

Conclusions

In summary, we described the synthesis of a novel electro-active poly(amic acid) containing oligoaniline pendants by one-step polycondensation. The obtained polymer shows good solubility, reversible electroactivity, and good electrochromic performance due to the existence of oligoaniline as the pendants. Moreover, due to the reversible acid–base doping–dedoping properties, the EPAA nanofibers exhibit acceptable gas sensing properties towards ammonia. Taking into account molecular diversity and tailoring, this type of electroactive polymer would be a highly promising candidate for gas sensors.

Acknowledgements

Notes and references

1 H. M. Zhang, X. H. Wang, J. Li, Z. S. Mo and F. S. Wang, *Polymer*, 2009, **50**, 2674–2679.
2 M. R. Anderson, B. R. Mattes, H. Reiss and R. B. Kaner, *Science*, 1991, **252**, 1412–1415.
3 B. Wessling and J. Posdorfer, *Electrochim. Acta*, 1999, **44**, 2139–2147.
4 L. B. Hu, G. Gruner, D. Li, R. B. Kaner and J. Cech, *J. Appl. Phys.*, 2007, **101**, 016102.
5 P. Camurlu, A. Cirpan and L. Toppare, *Mater. Chem. Phys.*, 2005, **92**, 413–418.
6 S. Koul, R. Chandra and S. K. Dhawan, *Polymer*, 2000, **41**, 9305–9310.
7 R. Faez, I. M. Martin, M. A. De Paoli and M. C. Rezende, *Synth. Met.*, 2001, **119**, 435–436.
8 H. L. Tai, Y. D. Jiang, G. Z. Xie, J. S. Yu, X. Chen and Z. H. Ying, *Sens. Actuators, B*, 2008, **129**, 319–326.
9 H. Bai, L. Zhao, C. H. Lu, C. Li and G. Q. Shi, *Polymer*, 2009, **50**, 3292–3301.
10 H. S. O. Chan, S. C. Ng, W. S. Sim, K. L. Tan and B. T. G. Tan, *Macromolecules*, 1992, **25**, 6029–6034.
11 P. N. Adams, D. C. Apperley and A. P. Monkman, *Polymer*, 1993, **34**, 328–332.
12 A. M. Kenwright, W. J. Feast, P. N. Adams, A. J. Milton, A. P. Monkman and B. J. Say, *Polymer*, 1992, **33**, 4292–4298.
13 L. H. Huang, X. L. Zhuang, J. Hu, L. Lang, P. B. Zhang, Y. Wang, X. S. Chen, Y. Wei and X. B. Jing, *Biomacromolecules*, 2008, **9**, 850–858.
14 T. C. Huang, T. C. Yeh, H. Y. Huang, W. F. Ji, Y. C. Chou, W. I. Hung, J. M. Yeh and M. H. Tsai, *Electrochim. Acta*, 2011, **56**, 10151–10158.
15 X. T. Jia, D. M. Chao, H. T. Liu, L. B. He, T. Zheng, X. J. Bian and C. Wang, *Polym. Chem.*, 2011, **2**, 1300–1306.
16 Z. M. Huang, Y. Z. Zhang, M. Kotaki and S. Ramakrishna, *Compos. Sci. Technol.*, 2003, **63**, 2223–2253.
17 D. Li and Y. N. Xia, *Adv. Mater.*, 2004, **16**, 1151–1170.

18 A. Greiner and J. H. Wendorff, *Angew. Chem., Int. Ed.*, 2007, **46**, 5670–5703.

19 Q. P. Pham, U. Sharma and A. G. Mikos, *Tissue Eng.*, 2006, **12**, 1197–1211.

20 C. Burger, B. S. Hsiao and B. Chu, *Annu. Rev. Mater. Res.*, 2006, **36**, 333–368.

21 C. P. Barnes, S. A. Sell, E. D. Boland, D. G. Simpson and G. L. Bowlin, *Adv. Drug Delivery Rev.*, 2007, **59**, 1413–1433.

22 D. Liang, B. S. Hsiao and B. Chu, *Adv. Drug Delivery Rev.*, 2007, **59**, 1392–1412.

23 J. W. Xie, X. R. Li and Y. N. Xia, *Macromol. Rapid Commun.*, 2008, **29**, 1775–1792.

24 E. Zampetti, S. Pantalei, S. Scalese, A. Bearzotti, F. De Cesare, C. Spinella and A. Macagnano, *Biosens. Bioelectron.*, 2011, **26**, 2460–2465.

25 Y. H. Li, J. Gong, G. H. He and Y. L. Deng, *Mater. Chem. Phys.*, 2011, **129**, 477–482.

26 X. H. Yu, X. G. Zhao, C. W. Liu, Z. W. Bai, D. M. Wang, G. D. Dang, H. W. Zhou and C. H. Chen, *J. Polym. Sci., Part A: Polym. Chem.*, 2010, **48**, 2878–2884.

27 P. Feng, X. Y. Xue, Y. G. Liu and T. H. Wang, *Appl. Phys. Lett.*, 2006, **89**, 342–345.

28 Y. X. Liang, Y. J. Chen and T. H. Wang, *Appl. Phys. Lett.*, 2004, **85**, 666–668.

29 T. Jeevananda, S. Siddaramaiah, S. Seetharamu, S. Saravanan and L. D'Souza, *Synth. Met.*, 2004, **140**, 247–260.

30 D. M. Chao, R. Yang, X. T. Jia, H. T. Liu, S. T. Wang, C. Wang and E. B. Berda, *J.Polym. Sci., Part A: Polym. Chem.*, 2012, **50**, 2330–2336.

31 Y. Furudawa, F. Ueda, Y. Hyodo and I. Harada, *Macromolecules*, 1988, **21**, 1297–1303.

32 M. Malta, E. R. Gonzalez and R. M. Torresi, *Polymer*, 2002, **43**, 5895–5901.

33 A. L. Kukla, Y. M. Shirshov and S. A. Piletsky, *Sens. Actuators, B*, 1996, **37**, 135–140.

34 V. V. Chabukswar, S. Pethkar and A. A. Athawale, *Sens. Actuators, B*, 2001, **77**, 657–663.

35 M. Matsuguchi, J. Io, G. Sugiyama and Y. Sakai, *Synth. Met.*, 2002, **128**, 15–19.

36 S. Wu, F. Zhang, F. Li and Y. Zhu, *Eur. Polym. J.*, 2000, **36**, 679–683.